Unusually Conductive Organic-Inorganic Hybrid Nanostructures Derived from Bio-Inspired Mineralization of Peptide/Pi-Electron Assemblies

Taein Lee, Sayak Subhra Panda, John D. Tovar, and Howard E. Katz

<u>Department of Materials Science and Engineering and Department of Chemistry, Johns Hopkins University, 3400 North Charles Street, Baltimore, MD 21218.</u> hekatz@jhu.edu

Abstract

Supramolecular materials derived from pi-conjugated peptidic macromolecules are wellestablished to self-assemble into 1-D nanostructures. In the presence of KOH that was used to more fully dissolve the peptide macromolecules prior to triggering the self-assembly by way of exposure to HCl vapor, we report here an unexpected mineralization of KCl as templated presumably by the glutamic acid residues that were present along the backbone of the peptide macromolecules. In order to decouple the peptidic side chains from the central pi-electron unit, 3carbon spacers were added between them on both sides. The assembled structures that resulted from the collective formation of β -sheets, π -orbital overlaps, and mineralization resulted in highly interconnected dendritic structures under suitable KOH concentrations. Electrical measurements indicated that when well-interconnected, these dendritic structures maintained conductivities comparable to those of metals at around 1800 S/cm. About 50 mA current was measured for 0.5 V/37.5 µm. Varying the gate voltage in a transistor configuration had no effect on the current levels, indicating a conductive instead of a semiconducting pathway. Control experiments without the peptide, measurements of conductivity over time, and conductivity quenching by ammonia suggested the conductivity of these dendritic networks was derived from proton doping of the central π -electron units in strong acid environment, and was facilitated by closely spaced chromophores as suggested in the literature leading to facile π -electron transfer along the interconnected dendritic pathways. Our findings suggest that mineralization templated by appropriate amino acids combined with peptide/ π -electron self-assembly can lead to highly conductive dendritic macrostructures as well as control of nanowire growth in specific directions.

Keywords: π -conjugation, peptide oligomer, self-assembly, mineralization, conductive nanowires

The high efficiency of charge-transport phenomena in biological systems^{1,2} has inspired numerous investigations into the conductivity of biologically relevant macromolecules processed from aqueous solution, as opposed to the well-established π -conjugated synthetic polymers and small organic molecules processed in toxic organic solvents.³⁻⁹ Among different biomacromolecules, self-assembling peptides and proteins attracted significant interest for development of chargetransporting materials 10-19 due to their ease of synthesis and tunable side chains to alter hierarchical organization that can impact conduction pathways. The use of synthetically modified polypeptides instead of natural proteins was explored to integrate the advantage of natural self-assembly and charge delocalizing properties of synthetic organic π -electron systems. ²⁰⁻²² While self-assembly of small synthetic peptides forming nanofibers and nanotubes has been exploited to form long-range conduction pathways, peptide-based π -conjugated materials emerged recently as active materials for devices such as field effect transistors and solar cells due to their ability to form robust 1D nanostructures with much more tunable electronic and photonic properties including significant hole conductivities and mobilities relative to purely peptidic materials. $^{23-33}$ π -Conjugated oligopeptides allow tuning of electrical and optoelectronic properties through incorporation of electron withdrawing and electron accepting chromophores within a polypeptide chain and through variation of the component amino acid residues.

Oligothiophenes and other organic semiconductor subunits are often the basis of π -conjugated peptides investigated for semiconducting properties, ³²⁻³⁴ but nanostructures derived from complex disk-like 2D π -electron structures such as benzotrithiophene and porphyrins with polypeptides have also been studied. ³⁵ We and others demonstrated significant hole mobilities in such species with the highest hole mobilities of 0.03 cm²V⁻¹s⁻¹ observed in a tripeptide-quaterthiophene-tripeptide system that could also transmit voltage and biases over macroscopic distances when used as a gate layer. ²⁹ Regardless of these advances, peptide-based charge transporting materials still suffer from relatively low conductivities compared to traditional organic semiconductor materials due to the substantial presence of 'insulating' peptidic regions. ^{29, 35-37} These problems pose a challenge for explicit characterization of the electrical transport pathways in biologically relevant materials and for consideration of any technological applications.

Here, we report our investigation of the morphologies and electrical properties of organic-inorganic hybrid self-assembled materials formed from peptide-spacer- π moieties and KCl. We investigated the 1D-nanostructures and electrical properties of materials formed from different proportions of the peptide, HCl, and KOH in aqueous solution. An acidic side chain amino acid (*i.e.* glutamic acid) was incorporated as the penultimate amino acid residue to control the pH-dependent self-assembly. In basic solution, the carboxylic acids of side chain amino acids are deprotonated and negatively charged, hindering the aggregation process *via* repulsion. On lowering pH to the acidic range, the carboxylate groups are protonated, neutralizing the charge, and allowing the peptides to self-assemble into well-defined nanostructures *via* H-bonding and π -chromophore quadrupolar interactions. The solution conditions fostered an apparent mineralization of KCl nanocrystals templated by the underlying peptide nanomaterial, a well-established process where ionized peptides locally sequester and concentrate metal ions prior to

their conversion into a variety of minerals.³⁸⁻⁴¹ We performed detailed structural and compositional characterizations of the nanostructures and measured their electrical conductivities in a bottom-gated two-terminal configuration.

Results and Discussion

In our previous design of the peptidic assembly, we had a carboxamide group directly attached to the π -core that could be expected to destabilize the radical cation formed during the hole-migration process. Here, we utilized a three-carbon alkyl spacer that we recently developed⁴² to separate the electrically active and self-assembling π -chromophore (*i.e.* phenyl-thiophene-phenyl) from the carboxamide group leading to a pentapeptide (**Figure 1a**). The spacers functioned to decouple the π -conjugated cores from the electron withdrawing carboxamide groups while maintaining the processability in aqueous solution. The 3-carbon spacer peptide was chosen for intensive investigation because it showed the most distinctive nanostructures and stability while providing sufficient decoupling between the chromophores and peptidic side chains.

There are three different reasons why this sequence was chosen: (a) The design of the peptides requires an acidic side-chain amino acid in the sequence which drives the assembly process under acidic condition due to charge screening. Hence, one (glutamic acid) of the two acidic side chain amino acid was chosen out of two options (glutamic acid and aspartic acid). (b) To maintain the water solubility of the molecules, highly hydrophobic sequences were not chosen near the pi-chromophore region, while peripheral valine residues were used to promote b-sheet structures. (c) We observed in our previous work^{26,30,42} that this sequence leads to formation of extended aggregates driven by beta-sheet type organization of the peptidic region as well as π -stacking in between the chromophores placing them close enough to undergo exciton coupling.

In general, alkyl groups are used to increase the solubility of organic semiconductors and promote their crystallization in organic solvents or on surfaces. However, for our peptides, they hindered the solubility of the molecules in aqueous solution at neutral pH. Ammonium hydroxide for example, did not fully dissolve the oligomers resulting in only self-assembly of the peptides during HCl exposure, leading to aggregates that were not connected and thus yielded no significant current (**Figure S1**). For that reason, we introduced KOH as a stronger base to ensure the solubility of the peptides. In the course of our experiments, we observed that different ionic compositions of these peptide solutions promote different structures upon self-assembly. Interestingly, we noticed dendritic (branched nanowire) growth of potassium chloride (KCl) in the presence of the peptides, where the organic structures acted as a template for the growth of inorganic phases. It was reported earlier that anionic groups in organic materials can concentrate inorganic cations leading to directed growth of crystalline solids, for example, forming bone-like structures.⁴¹

Dendritic nanowire structure and mineralization. As aforementioned, a small amount of KOH was added to make the molecular peptide soluble prior to assembly rather than beginning the assembly with suspended aggregates. ^{26, 29, 43, 44} The initial concentration of the peptide was 1 wt% in water. The peptide mixed with water initially formed a turbid solution at room temperature. The KOH added, from a 1M stock solution, was double the mass of the peptide in the solution. We did not observe formation of crystals in solution upon addition of KOH prior to evaporation. KCl crystals seemed to grow around the dendritic fibrils of peptides during the acidification process caused by the diffusion of hydrochloric acid vapor (Figure 2). We hypothesize that upon addition of KOH, the negative charge on the glutamic acid attracts K⁺ ions and, and then in the presence of HCl vapor, K⁺ binds with Cl⁻ to form KCl structures. This can be

correlated to the idea of biomineralization, which is a commonly observed phenomenon in which glutamic and aspartic acids act to sequester and locally concentrate metal ions.⁴⁵

Compositional analysis using scanning electron microscopy / energy dispersive X-ray spectroscopy (SEM/EDS) of a region in between gold electrodes for electrical measurement (Figure 1b) supported the idea of mineralization during self-assembly (Figure 3). Energy Dispersive X-ray Spectroscopy is a technique used along with SEM to understand compositional analysis of the sample. In general, a particular area of the sample is bombarded with electron beam and energy of the X-rays emitted from the sample were detected to figure out the elemental composition of the sample from area of interest. The energy of the emitted x-ray is plotted in xaxis along with the intensity of the X-ray in y-axis. The presence of K, Cl, S and Si in Spot 1 proves growth of KCl using the self-assembling peptidic structures as a template, whose presence is proved by S, the heaviest element in the peptide pi-conjugated molecules (Figure 3d). On the other hand, only Si is observed in Spot 2 indicating most of the peptide molecules are assembled into the dendritic regions and KCl shells form around them in a Volmer-Weber type growth mode (Figure 3e). The presence of gold only in electrode regions (Figure 3d, 3e) and its absence between electrodes rule out the possibility of conduction, observed in experiments to be discussed next, via gold interconnections (Figure 3f, 3g). As SEM/EDS has higher intensity count for heavier elements, the presence of Au as well as K and Cl in Spot 4 masked the peak for S (Figure 3g). Without any peptide molecules, KOH only forms block KCl crystals under HCl vapor exposure (Figure S2, including a KCl x-ray diffraction peak), supporting the idea that these peptidic nanostructures are acting as templates to form well-defined dendritic KCl superstructures. Initiation sites with critical nuclei sizes followed by the subsequent growth of KCl, coupled with self-assembling nanowire structures from beta-sheet-like hydrogen bond network formation

among peptide sequences and π -stacking of the central chromophores, lead to nanowire growth, as reported previously for similar peptidic structures.^{26,29} These types of structures were not observed when ammonium hydroxide was used instead of KOH as the base (**Figure S1**). Thus, nucleation and growth of self-assembled structures were accompanied by KCl mineralization in a coordinated process during Volmer-Weber type growth of peptides.⁴¹

Concentrations of peptides were varied from 0.0015 to 0.015M, corresponding to 0.2 to 2 wt. %, while keeping the same procedures for pH-triggered self-assembly to investigate the effect on structure and corresponding electrical properties. A summary observation of the drop-casted samples was that there was some form of dendrite of varying length and thickness for all samples (Figure 4). Kinetically relevant factors such as the amount of peptide and KOH during the self-assembly and mineralization processes dictated the resulting dendritic structures. For example, a higher KOH amount in 0.015M samples, upon exposure to HCl vapor, facilitated formation and growth of KCl leading to KCl block crystals. In such cases, the peptides were in the surroundings (Figures S3 and S4). Hence, a right balance of KOH and peptide concentration was imperative for coordinated growth of connected dendrite complex composed of peptides encapsulated in KCl, under constant HCl exposure times.

Laser optical and 3D images at 100x magnification of peptides with varying concentrations showed different structures for each concentration. 0.0015 to 0.0057M samples had disconnected dendrites due to insufficient amount of peptides and KCl unable to fully connect with other nucleating sites of self-assembly and KCl formation (**Figures 5a, 5b, 5c**). 0.0068 to 0.0076M samples had appropriate ratios of KOH and peptides, enabling formation of well-connected dendrites (**Figures 5d, 5e**). 0.0095 to 0.015M samples showed less dendrite coverage and instead larger blocks of KCl with increasing concentration (**Figures 5f, 5g, 5h**); More KOH was required

to dissolve the higher concentration of peptides, resulting in KCl mineralizing faster than self-assembly of the peptides, leading to formation of blocks of KCl. Higher concentration also led to aggregation, further facilitating the mineralization of KCl block crystals before peptides could self-assemble into dendrites for 0.0095 to 0.015M samples (**Figures 5f, 5g, 5h**).

Dependence of electrical performance on structure. The presence of interconnected dendritic structure was the most critical factor for conductivity.⁵³ The 3D laser microscope images show that only 0.0068 and 0.0076M samples had connected dendrites (Figures 5d, 5e). This corresponds to the electrical data for which only 0.0068M and 0.0076M samples showed significant conductance (Figures 6 and 7) and essentially no conductance at all for all other concentrations, even at higher voltage bias (Figure S5). The current measurements for 0.0068 and 0.0076M samples had conductivity lower than, but comparable to those of metals. There was no gate effect, as can be seen from the current at a range of gate voltages shown in Figures 6 and 7, respectively. (We continue to plot currents *vs.* gate voltage to illustrate the lack of gate effect in our samples.) Samples prepared with peptides dissolved in KOH without HCl vapor exposure had no dendritic formation and no conductance, further highlighting the importance of connected dendritic structure for conductive pathway formation (Figure S6).

Conductivity of each connected dendrite was calculated under the assumption that the dendrite has ohmic conduction. Using Ohm's law and the conductance formula for a wire with a defined cross-sectional area and length, the conductivity was calculated to be around 1800 S/cm for a 0.0076M sample with a well-connected network of dendrites. The calculations and dimensions used for calculations are described in supplementary information (**Figure S7** and **S8**). This conductivity is comparable to that of some metallic materials in less conductive forms and highly conductive biological materials in aqueous media. 46-49

Having ruled out the possibility of conduction *via* gold from SEM/EDS where no gold was observed between electrodes, we needed to consider whether the KCl formed by the mineralization process could have been the conductive medium. KCl formed between electrodes from only KOH solution exposed to HCl vapor showed no current under the same conditions, demonstrating that KCl cannot be the medium of the current pathway (**Figures S2**, **S9**). Further, a timed test showed 60% retention of the current after 5000s of -0.5 Vd applied continuously without gate voltage bias for 0.0076M sample, indicating most of the conductivity is from electron/hole conduction (**Figure 8**). The integrated transported charge was much higher than the total number of mobile ions present in the conductive region, consistent with electronic/hole conduction as the primary conduction mechanism instead of ionic conduction. Ionic conduction also would have decreased much more rapidly at this current level due to accumulation of ions at the electrodes and the resulting ionic repulsion. This leaves the structural arrangement of the peptides in the dendrites with mineralized KCl shells as the reason for the abnormally high conductivity.

We suggest that fixation of π -stacked organic semiconductor subunits in a conductive morphology was achieved by overlap of multiple KCl crystals from multiple heterogeneous sites (**Figure 2b**), which has been observed before in biomineralization.⁵⁰ Multiple KCl crystals mineralizing simultaneously with β -sheet formation from intermolecular peptide interactions such as hydrogen bonding between amino acids, and sulfur-sulfur contacts between thiophene groups²⁶, could have allowed closer than normal packing of peptides. In addition, the π -electron units within the peptide nanostructures could have been doped by protons because π -conjugated organic polymers are known to have high capacity for proton doping in the presence of strong acids like HCl, which contributes to increasing conductivity and enhancing self-assembly.⁵¹⁻⁵⁵ The decoupling of the electron withdrawing peptide amide groups from the chromophores by the 3-

carbon spacer further promoted this protonic acid doping.⁵⁵ Altogether, we conclude that the facile current flow with stacked layers of proton doped chromophores with Cl- counter ions from the excess HCl, with charge possibly screened by interactions with KCl crystallites, induced a high hole density within assemblies of closely packed chromophores.

Proton doping on chromophores achieved by HCl was consistent with an observed decrease in current output upon exposure of a well interconnected 0.0076M sample to ammonium hydroxide, which functioned as a de-doping agent for the proton doped chromophores (Figure 9).^{51,52} Analyzing the directionality and distance effect on the conductivity of dendrites further indicated conductive wire-like resistance. Decreasing conductivity with increasing distance indicated the dendrites are functioning as a wire with resistance (Figure 10). Well interconnected dendrites formed conductive pathways throughout the whole sample for over 1.5 mm in length for 17 spacings (calculated from Figure S7) and had varying conductances according to position of electrodes on the sample (Figures S10, 11, 12) indicating non-uniform current path formation throughout the sample as expected of self-assembled structures. Some samples with partially connected dendrites with slightly lower concentrations also showed currents (Figure S13). However, the quick degradation of conductive pathway, the response to humidity, and the significantly lower current output than that of the connected dendrites all indicated that these currents from partially connected dentrites are ionic in nature (Figure S13). Even at the highest output, ionic conduction from the amino acid side chains of slightly connected dendrites was insignificant compared to electron/hole conduction current levels. Hence, both electronic and ionic conduction pathways exist for the connected dendrites, but electronic conduction pathway appears to be dominant, once the pathway forms.

Due to the stability provided by the KCl shells, well-formed conductive pathways of 0.0076M samples were intact for weeks before losing around 90% of their conductivity after 43 days under ambient environment as shown in **Figure 11 and Figure S14**. During this time, current output degraded slowly over time, possibly due to repelling force between doped π -stacked regions to regain equilibrium distance and/or deactivation/dissipation of the hypothesized doping protons, which was delayed by the KCl shell surrounding the nanowires. These factors disoriented the closely packed and fixated arrangements of peptides in KCl shells over time, allowing them to slowly readjust to normal distance and with further disintegration of structure and dissipation of doped protons, to eventually lose the vital structural arrangement for high conductivity.

Conclusion

Dendritic structures assembled *via* connection between mineralizing KCl crystallites initiated by pH-triggered self-assembly of peptide materials was demonstrated in this work. Connected structures were found to be the most important factor to producing highly conductive nanowire assemblies that showed conductivity comparable to that of a metal. It was found that the dominant conduction mechanism of samples with well-connected dendrite structures is electronic conduction. We hypothesize that this arose from proton doped chromophores with Cl- counter ions from excess HCl vapor stacking in closer-than-normal proximity with the aid of mineralized KCl encasing the side chains of the oligopeptides. The results presented here demonstrate a different approach to self-assembly followed by mineralization to achieve structures with high electrical conductivity. They suggest that other more electronically relevant materials may be subject to templation by these hybrid bio/pi-electron materials and will be explored in the future.

Experimental section

Peptide Synthesis. All polymers were synthesized and prepared according to our recently accepted publication. All other reagents and starting materials were obtained from Sigma-Aldrich and were used as received.

Scanning Electron Microscopy / **Energy Dispersive X-ray Spectroscopy.** All samples were observed under Tescan MIRA 3 GMU for all SEM images at 20 KeV for working distance between 10 and 30 mm. All EDS data was acquired *via* and AMATEK EDAX Octane Plus.

3D Laser Scanning Microscopy. In order to assess the formation of structures that were formed, all 3D and laser microscope images were acquired *via* a Keyence VK-X 100 laser microscope.

Device Fabrication and Measurements. The devices were fabricated on silicon substrates acquired from University Wafers with diameter 150mm with 300 nm SiO₂, a capacitance per area of 11.5 nF/cm², and in the <100> orientation. The substrates were cleaned in piranha (2:1 ratio of concentrated sulfuric acid to hydrogen peroxide) for 3 hours, rinsed with DI water for 10 minutes, sonicated in acetone for 20 minutes, rinsed with DI water for 10 minutes, and sonicated in 2-propanol for 20 minutes before cleaning the substrate by blowing dry nitrogen gas. Solutions of the polymer were dropped on the substrates and immediately exposed to HCl vapor from a vial full of concentrated HCl (directly from the original bottle) using a glass lid to encase both the HCl vial and substrate for 5 minutes in a chamber before removing the sample from the chamber and letting it dry. After drying for one day, 50 nm of gold was evaporated onto the samples at a rate of 0.4Å/s with an Edwards 306 evaporator using a 200 mesh TEM grid for electrical measurements. A Keithley semiconductor analyzer was used for all electrical measurements.

Supporting Information Available: The content in supporting information includes SEM and 3D laser optical microscope images of various control experiments as well as SEM/EDS data for elemental analysis of the structures that formed. Electrical measurement data for control samples and controlled electrical measurement data as well as images, conditions, and assumptions for conductivity calculations are also included in the supporting information file. This material is available free of charge *via* the Internet at http://pubs.acs.org.

Acknowledgments. This work was supported by the National Science Foundation DMREF program, grant number DMR-1728947. All of the images in figures and ToC graphics were created entirely by the authors.

References

- 1. Winkler, J. R; Gray, H. B. Electron Transfer in Ruthenium-Modified Proteins. *Chem. Rev.* **1992**, *92*, 369-379.
- 2. Gray, H. B.; Winkler, J. R. Electron Transfer in Proteins. *Annu. Rev. Biochem.* **1996**, *65*, 537–561.
- 3. Chworos, A.; Severcan, I.; Koyfman, A. Y.; Weinkam, P.; Oroudjev, E.; Hansma, H. G.; Jaeger, L. Building Programmable Jigsaw Puzzles with RNA. *Science* **2004**, *306*, 2068–2072.
- 4. Ordinario, D. D.; Phan, L.; Walkup IV, W. G.; Jocson, J-M.; Karshalev, E.; Hüsken, N.; Gorodetsky, A. A. Bulk Protonic Conductivity in a Cephalopod Structural Protein. *Nat. Chem.* **2014**, *6*, 596–602.
- 5. Aida, T.; Meijer, E. W.; Stupp, S. I. Functional Supramolecular Polymers. *Science* **2012**, *335*, 813–817.
- 6. Panda, S. S.; Katz, H. E.; Tovar, J. D. Solid-State Electrical Applications of Protein and Peptide Based Nanomaterials. *Chem. Soc. Rev.* **2018**, *47*, 3640-3658.
- 7. Tseng, P.; Napier, B.; Zhao, S. W.; Mitropoulos, A. N.; Applegate, M. B.; Marelli, B.; Kaplan, D. L.; Omenetto, F. G. Directed Assembly of Bio-Inspired Hierarchical Materials with Controlled Nanofibrillar Architectures. *Nat. Nanotechnol.* **2017**, *12*, 474-480.

- 8. Lovley, D. R. Electrically Conductive Pili: Biological Function and Potential Applications in Electronics. *Curr. Opin. Electrochem.* **2017**, *4*, 190–198.
- 9. Wang, L. L.; Jackman, J. A; Ng, W. B.; Cho, N. J. Flexible, Graphene-Coated Biocomposite for Highly Sensitive, Real-Time Molecular Detection. *Adv. Funct. Mater.* **2016**, *26*, 8623–8630.
- 10. Amit, M.; Yuran, S.; Gazit, E.; Reches, M.; Ashkenasy, N. Tailor-Made Functional Peptide Self-Assembling Nanostructures. *Adv. Mater.* **2018**, *30*, 1707083.
- 11. Ghadiri, M. R.; Granja, J. R.; Milligan, R. A.; McRee, D. E.; Khazanovich, N. Self-Assembling Organic Nanotubes Based on a Cyclic Peptide Architecture. *Nature* **1994**, *366*, 324–327.
- 12. Jatsch, A.; Schillinger, E. K.; Schmid, S.; Baeuerle, P. Biomolecule Assisted Self-Assembly of Pi-Conjugated Oligomers. *J. Mater. Chem.* **2010**, *20*, 3563–3578.
- 13. Ing, N. L.; El-Naggar, M. Y.; Hochbaum, A. I. Going the Distance: Long-Range Conductivity in Protein and Peptide Bioelectronic Materials. *J. Phys. Chem. B* **2018**, *122*, 10403-10423.
- 14. Kumar, M.; Ing, N. L.; Narang, V.; Wijerathne, N.; Hochbaum, A. I.; Ulijn, R. V. Amino Acid-Encoded Biocatalytic Self-Assembly Enables the Formation of Transient Conducting Nanostructures. *Nat. Chem.* **2018**, *10*, 696-703.
- 15. Sepunaru, L.; Pecht, I.; Sheves, M.; Cahen, D. Solid-State Electron Transport Across Azurin: from a Temperature-Independent to a Temperature-Activated Mechanism. *J. Am. Chem. Soc.* **2011**, *133*, 2421–2423.
- 16. Amit, M.; Appel, S.; Cohen, R.; Cheng, G.; Hamley, I. W.; Ashkenasy, N. Hybrid Proton and Electron Transport in Peptide Fibrils. *Adv. Funct. Mater.* **2014**, *24*, 5873–5880.
- 17. Stone, D. A.; Hsu, L.; Stupp, S. I. Self-Assembling Quinquethiophene-Oligopeptide Hydrogelators. *Soft Matter* **2009**, *5*, 1990–1993.
- 18. Diegelmann, S. R.; Gorham, J. M.; Tovar, J. D. One-Dimensional Optoelectronic Nanostructures Derived from the Aqueous Self-Assembly of Pi-Conjugated Oligopeptides. *J. Am. Chem. Soc* **2008**, *130*, 13840–13841.
- 19. Kumar, R. J.; MacDonald, J. M.; Singh, T. B.; Waddington, L. J.; Holmes, A. B. Hierarchical Self-Assembly of Semiconductor Functionalized Peptide Alpha-Helices and Optoelectronic Properties. *J. Am. Chem. Soc.* **2011**, *133*, 8564–8573.
- 20. Del Mercato, L. L.; Pompa, P. P.; Maruccio, G.; Della Torre, A.; Sabella, S.; Tamburro, A. M.; Cingolani, R.; Rinaldi, R. Charge Transport and Intrinsic Fluorescence in Amyloid-Like Fibrils. *Proc. Natl. Acad. Sci. U. S. A.* **2007**, *104*, 18019–18024.
- 21. Amit, M.; Ashkenasy, N. Electronic Properties of Amyloid β Based Peptide Filaments with Different Non-Natural Heterocyclic Side Chains. *Isr. J. Chem.* **2014**, *54*, 703–707.
- 22. Ashkenasy, N.; Horne, W. S.; Ghadiri, M. R. Design of Self-Assembling Peptide Nanotubes with Delocalized Electronic States. *Small* **2006**, *2*, 99–102.
- 23. Tovar, J. D. Supramolecular Construction of Optoelectronic Biomaterials. *Acc. Chem. Res.* **2013**, *46*, 1527–1537.

- 24. Ardona, H. A. M.; Tovar, J. D. Peptide π-Electron Conjugates: Organic Electronics for Biology? *Bioconjugate Chem.* **2015**, *26*, 2290–2302.
- 25. Khalily, M. A.; Bakan, G.; Kucukoz, B.; Topal, A. E.; Karatay, A.; Yaglioglu, H. G.; Dana, A.; Guler, M. O. Fabrication of Supramolecular *n/p*-Nanowires *via* Coassembly of Oppositely Charged Peptide-Chromophore Systems in Aqueous Media. *ACS Nano* **2017**, *11*, 6881–6892.
- 26. Wall, B. D.; Diegelmann, S. R.; Zhang, S.; Dawidczyk, T. J.; Wilson, W. L.; Katz, H. E.; Mao, H.-Q.; Tovar, J. D. Aligned Macroscopic Domains of Optoelectronic Nanostructures Prepared *via* Shear-Flow Assembly of Peptide Hydrogels. *Adv. Mater.* **2011**, *23*, 5009–5014.
- 27. Ardona, H. A. M.; Besar, K.; Togninalli, M.; Katz, H. E.; Tovar, J. D. Sequence-Dependent Mechanical, Photophysical and Electrical Properties of Pi-Conjugated Peptide Hydrogelators. *J. Mater. Chem. C* **2015**, *3*, 6505–6514.
- 28. Eakins, G. L.; Pandey, R.; Wojciechowski, J. P.; Zheng, H. Y.; Webb, J. E. A.; Valery, C.; Thordarson, P.; Plank, N. O. V.; Gerrard, J. A.; Hodgkiss, J. M. Functional Organic Semiconductors Assembled via Natural Aggregating Peptides. *Adv. Funct. Mater.* **2015**, *25*, 5640–5649.
- 29. Besar, K.; Ardona, H. A. M.; Tovar, J. D.; Katz, H. E. Demonstration of Hole Transport and Voltage Equilibration in Self Assembled π -Conjugated Peptide Nanostructures Using Field-Effect Transistor Architectures. *ACS Nano* **2015**, *9*, 12401–12409.
- 30. Sanders, A. M.; Dawidczyk, T. J.; Katz, H. E.; Tovar, J. D. Peptide-Based Supramolecular Semiconductor Nanomaterials *via* Pd-Catalyzed Solid-Phase "Dimerizations". *ACS Macro Lett.* **2012**, *1*, 1326–1329.
- 31. Draper, E. R.; Lee, J. R.; Wallace, M.; Jackel, F.; Cowan, A. J.; Adams, D. J. Self-Sorted Photoconductive Xerogels. *Chem. Sci.*, **2016**, *7*, 6499–6505.
- 32. Tsai, W-W.; Tevis, I. D.; Tayi, A. S.; Cui, H.; Stupp, S. I. Semiconducting Nanowires from Hairpin-Shaped Self-Assembling Sexithiophenes. *J. Phys. Chem. B* **2010**, *114*, 14778–14786.
- 33. Aida, T.; Meijer, E. W.; Stupp, S. I. Functional Supramolecular Polymers. *Science* **2012**, 335, 813–817.
- 34. Horowitz, G. Organic Field-Effect Transistors. Adv. Mater. 1998, 10, 365–377.
- 35. Sun, Y.; Jiang, L.; Schuermann, K. C.; Adriaens, W.; Zhang, L.; Boey, F. Y. C.; De Cola, L.; Brunsveld, L.; Chen, X. Semiconductive, One-Dimensional, Self-Assembled Nanostructures Based on Oligopeptides with π-Conjugated Segments. *Chem. Eur. J.* **2011**, *17*, 4746–4749.
- 36. Prasanthkumar, S.; Gopal, A.; Ajayaghosh, A. Self-Assembly of Thienylenevinylene Molecular Wires to Semiconducting Gels with Doped Metallic Conductivity. *J. Am. Chem. Soc.* **2010**, *132*, 13206–13207.
- 37. Sanders, A. M.; Kale, T. S.; Katz, H. E.; Tovar, J. D. Solid-Phase Synthesis of Self-Assembling Multivalent Pi-Conjugated Peptides. *ACS Omega* **2017**, *2*, 409–419.
- 38. Hartgerink, J. D.; Beniash, E.; Stupp, S. I. Self-Assembly and Mineralization of Peptide-Amphiphile Nanofibers. *Science* **2001**, *294*, 1684–1688.
- 39. Aizenberg, J.; Muller, D. A.; Grazul, J. L.; Hamann, D. R. Direct Fabrication of Large Micropatterned Single Crystals. *Science* **2003**, *299*, 1205–1208.
- 40. Estroff, L. A. Introduction: Biomineralization. Chem. Rev. 2008, 108, 4329–4331.

- 41. Weiner, S.; Addadi, L. Crystallization Pathways in Biomineralization. *Ann. Rev. Mat. Res.* **2011**, *41*, 21-40.
- 42. Panda, S. S.; Shmilovich, K.; Ferguson, A. L.; Tovar, J. D. Controlling Supramolecular Chirality in Peptide-π-Peptide Networks by Variation of the Alkyl Spacer Length. *Langmuir* **2019**, *35*, 14060–14073.
- 43. Omosun, T. O.; Hsieh, M-C.; Childers, W. S.; Das, D.; Mehta, A. K.; Anthony, N. R.; Pan, T.; Grover, M. A.; Berland, K. M.; Lynn, D. G. Catalytic Diversity in Self-Propagating Peptide Assemblies. *Nat. Chem.* **2017**, *9*, 805-809.
- 44. Stupp, S. I.; Palmer, L. C. Supramolecular Chemistry and Self-Assembly in Organic Materials Design. *Chem. Mater.* **2014**, *26*, 507-518.
- 45. Eiden-Aßmann, S.; Viertelhaus, M.; Heiß, A.; Hoetzer, K. A.; Felsche, J. The Influence of Amino Acids on the Biomineralization of Hydroxyapatite in Gelatin. *J. Inorg. Biochem.* **2002**, *91*, 481-486.
- 46. Cohen, M. J.; Coleman, L. B.; Garito, A. F.; Heeger, A. J. Electrical Conductivity of Tetrathiofulvalinium Tetracyanoquinodimethan (TTF) (TCNQ). *Phys. Rev. B.* **1974**, *10*, 1298–1307.
- 47. Walsh, F. C. Electrode Reactions in Metal Finishing. *Transactions of the IMF* **1991**, *69*, 107–110.
- 48. Ing, N. L.; Spencer, R. K.; Luong, S. H.; Nguyen, H. D.; Hochbaum, A. I. Electronic Conductivity in Biomimetic α-Helical Peptide Nanofibers and Gels. *ACS Nano*, **2018**, *12*, 2652–2661.
- 49. Tsakiris, V.; Kappel, W.; Alecu, G. Solid State Diffusion Welding of Cu-Fe/Al/Ag and Al-Ni Dissimilar Metals. *J. Optoelectron. Adv. M.* **2011**, *13*, 1176-1180.
- 50. Kabalah-Amitai, L.; Mayzel, B.; Kauffmann, Y.; Fitch, A. N.; Bloch, L.; Gilbert, P. U. P. A.; Pokroy, B. Vaterite Crystals Contain Two Interspersed Crystal Structures. Science **2013**, *340*, 454-457.
- 51. MacDiarmid, A. G. "Synthetic Metals": A Novel Role for Organic Polymers. *Angew. Chem., Int. Ed.*, **2001**, *40*, 2581-2590.
- 52. Ma, Z.; Shi, W.; Yan, K.; Pan, L.; Yu, G. Doping Engineering of Conductive Polymer Hydrogels and Their Application in Advanced Sensor Technologies. *Chem. Sci.* **2019**, *10*, 6232-6244.
- 53. Außerlechner, S. J.; Gruber, M.; Hetzel, R.; Flesch, H.; Ladinig, L.; Hauser, L.; Hause, A.; Buchner, M.; Resel, R.; Schurrer, F.; Stadlober, B.; Trimmel, G.; Zojer, K.; Zojer, E. Mechanism of Surface Proton Transfer Doping in Pentacene Based Organic Thin-Film Transistors. *Phys. Stat. Sol. A.* **2012**, *209*, 181–192.
- 54. Lussem, B.; Keum, C-M.; Kasemann, D.; Naab, B.; Bao, Z.; Leo, K. Doped Organic Transistors. *Chem. Rev.* **2016**, *116*, 13714-13751.
- 55. Miller, L. L.; Mann, K. R. π-Dimers and π-Stacks in Solution and in Conducting Polymers. *Acc. Chem. Res.* **1996**, *29*, 417-423.

Main Figures

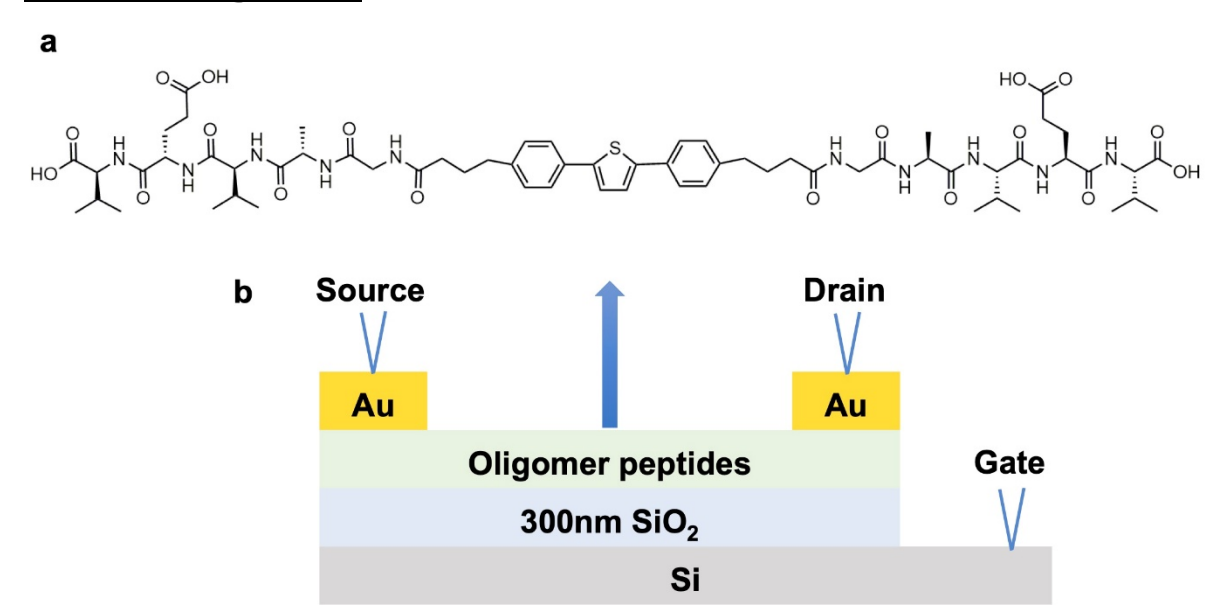


Figure 1. (a) Chemical structure of peptide-spacer- π molecule. (b) Field-Effect Transistor (FET) set-up for electrical measurements.

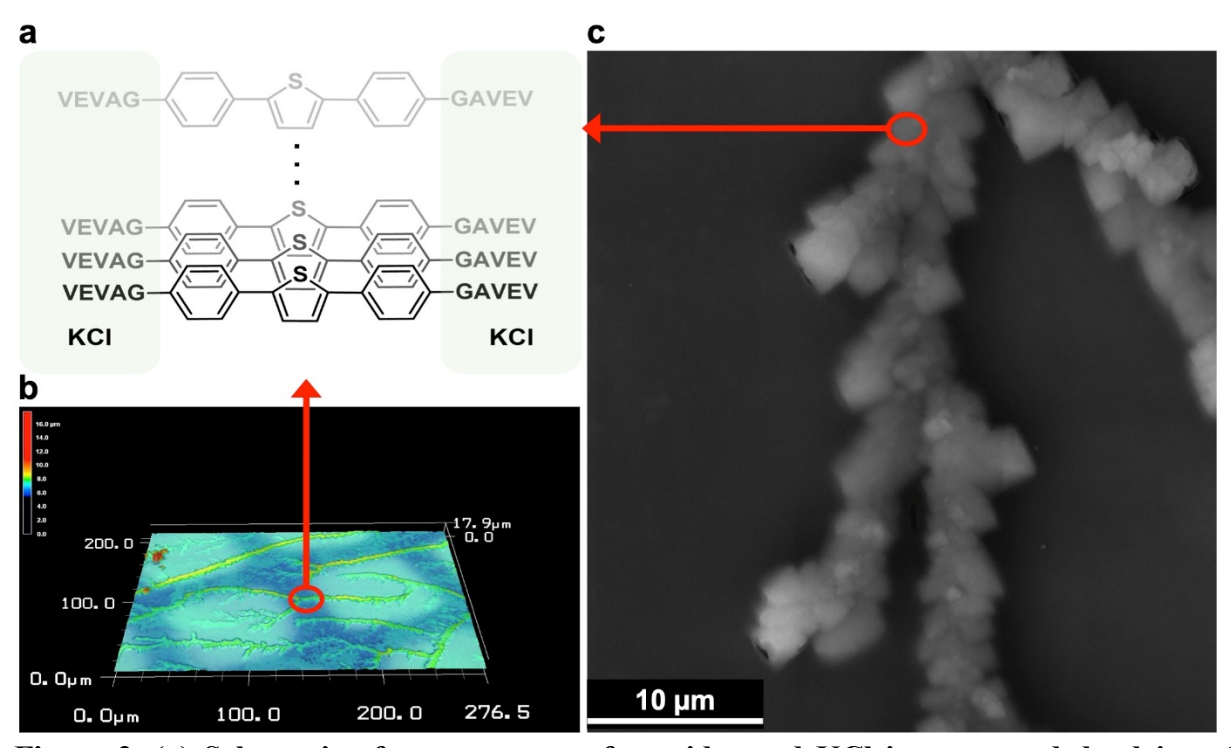


Figure 2. (a) Schematic of arrangement of peptides and KCl in connected dendrites. (b) Connected dendrite images at 50x magnification of 0.0076M sample under laser microscope. (c) SEM image of 0.0076M sample at 7.70kx magnification.

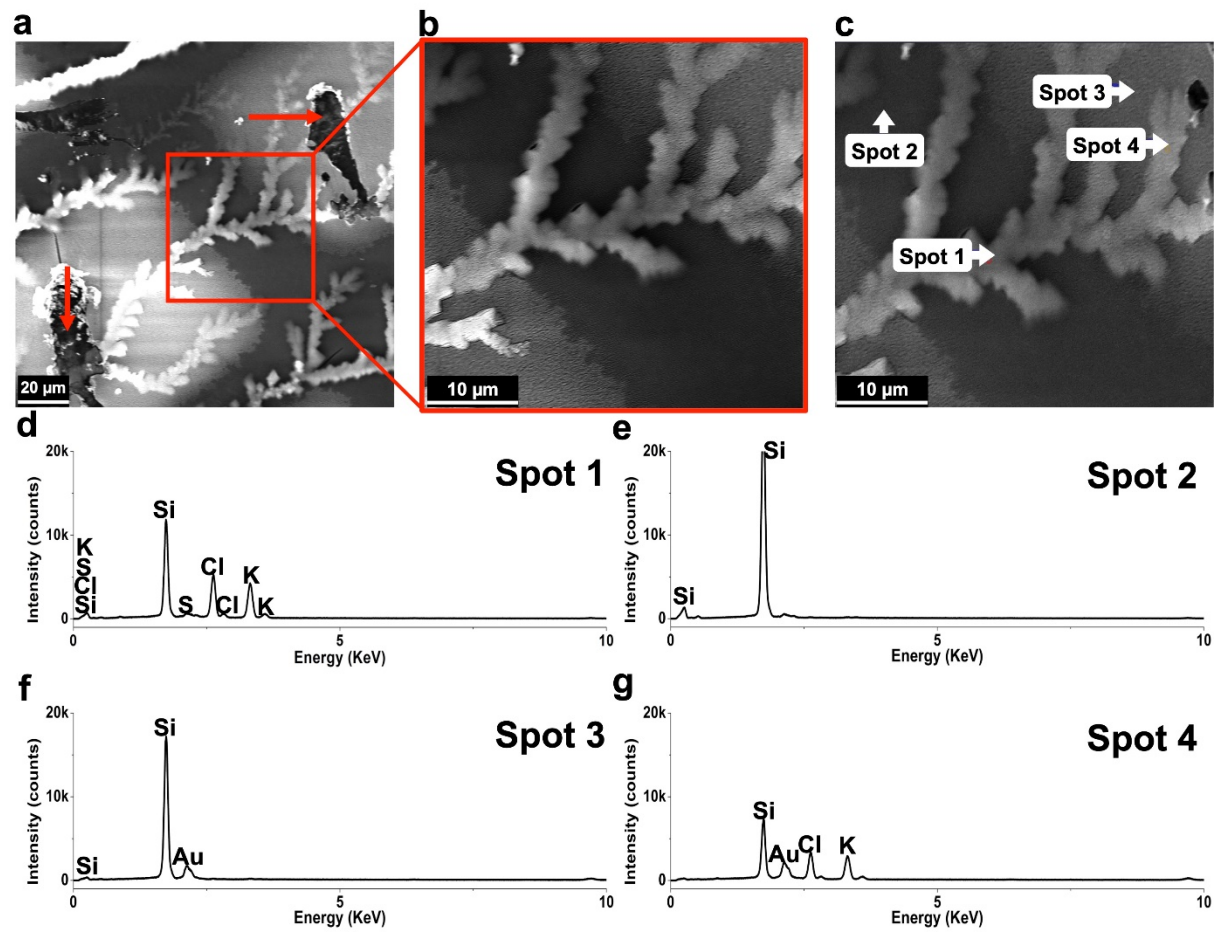


Figure 3. SEM images and related SEM EDAX data for different regions on sample. (a) SEM image of 0.0076M at 1.81kx magnification for a region in between electrically tested areas, shown by the arrows. (b) SEM image of dendrite region in between the Au electrodes indicated by the red box in (a) at 4.73kx magnification. (c) The 4 different spots SEM EDAX was performed is shown. (d) SEM EDAX of spot 1 where there is only dendrite on Si/SiO₂ wafer. (e) SEM EDAX of spot 2 where there is no assembly of dendrite on Si/SiO₂ wafer. (f) SEM EDAX of spot 3 where there is only Au on Si/SiO₂ and no assembly of dendrite. (g) SEM EDAX of spot 4 of dendrite on Si wafer below Au.

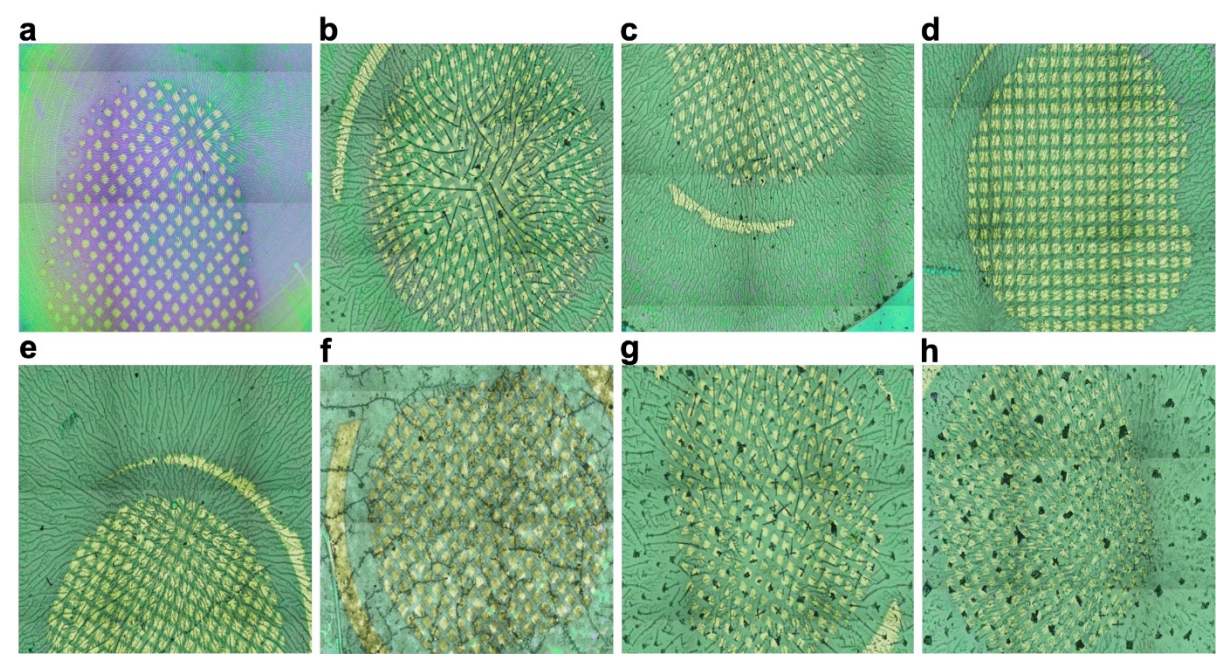


Figure 4. Stitched holistic view of the samples under laser microscope at 10x magnification for sample with (a) 0.0015M, (b) 0.0038M, (c) 0.0057M, (d) 0.0068M, (e) 0.0076M, (f) 0.0095M, (g) 0.011M, and (h) 0.015M peptides. More KOH to dissolve the higher amount of oligomers in 0.0095M to 0.015M samples lead to more formation of KCl salt crystals, resulting in block crystals. Gold squares are 37.5 µm apart.

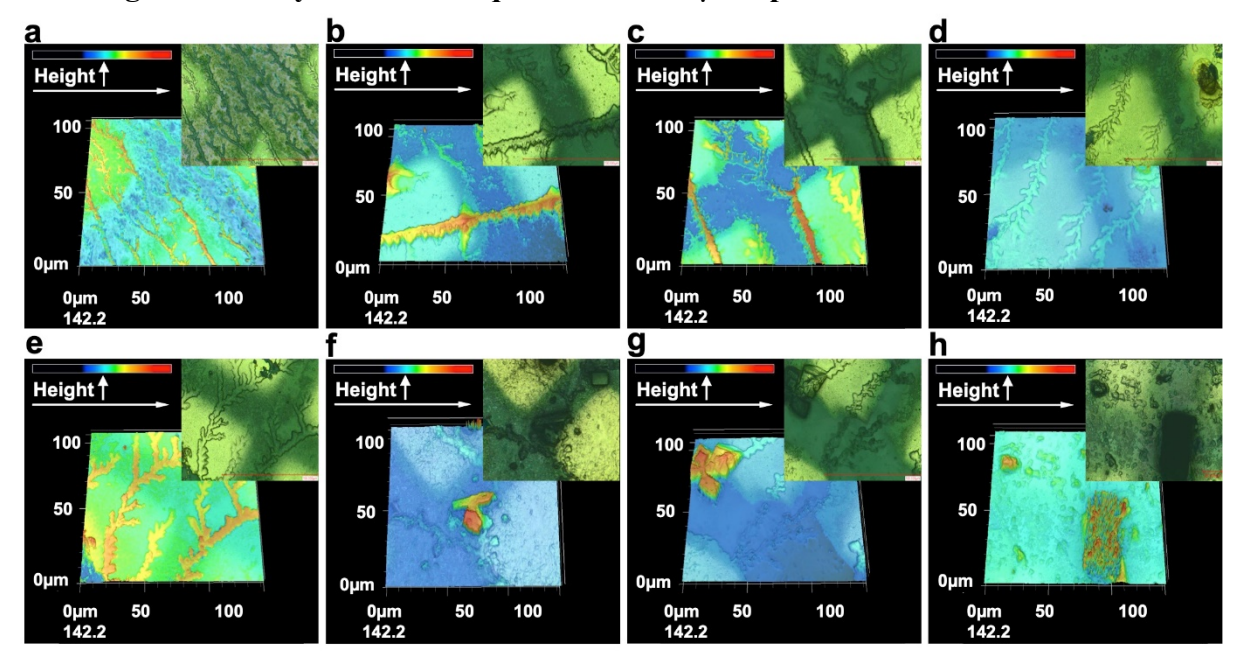


Figure 5. 3D images of dendrites between Au electrodes with inset of optical images, both at 100x magnification under laser microscope for (a) 0.0015M, (b) 0.0038M, (c) 0.0057M, (d) 0.0068M, (e) 0.0076M, (f) 0.0095M, (g) 0.011M, and (h) 0.015M samples.

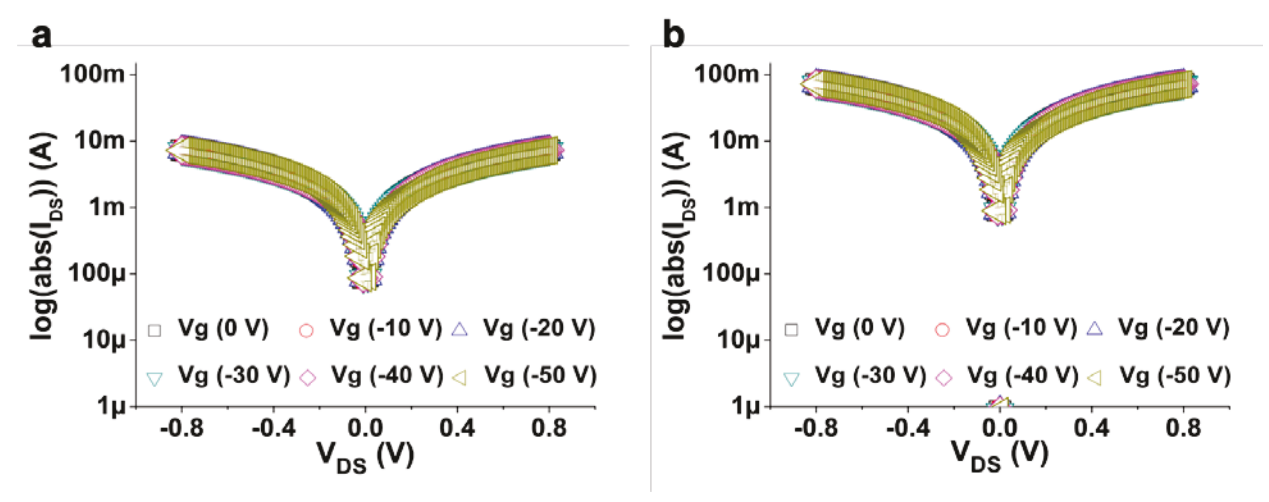


Figure 6. Averaged current over range of voltages with error bars for Vd from 0 to -1 V in -0.2 V steps and for Vg from 0 to -50 V for (a) 0.0068M and (b) 0.0076M. Other than 0.0068 and 0.0076M samples, no samples showed significant current.

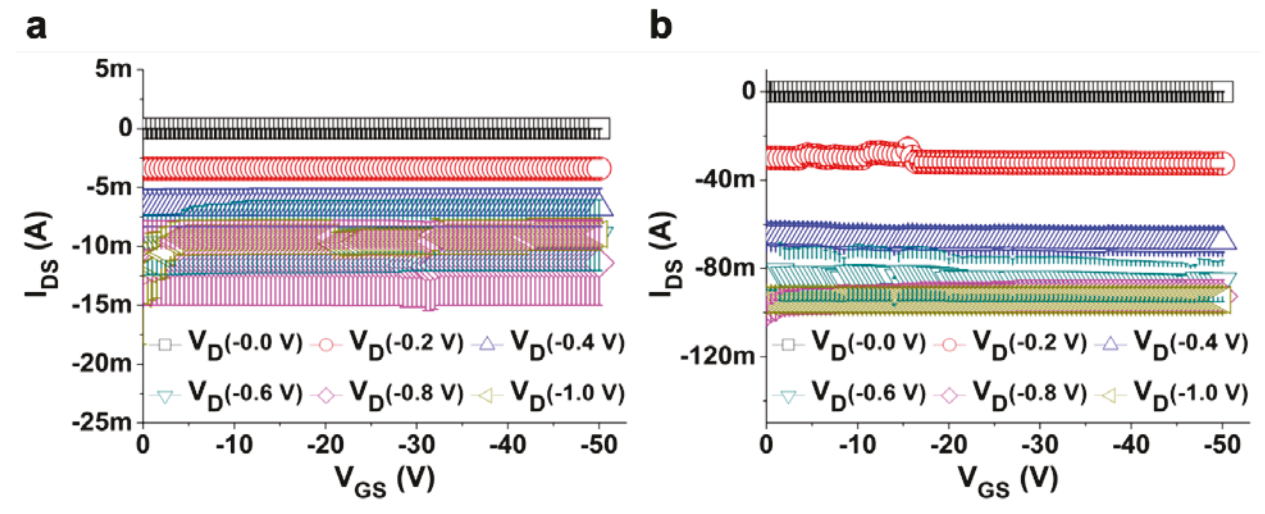


Figure 7. Averaged current over range of voltages with error bars for Vg from 0 to -50 V in -0.5 V steps and for Vd from -50 to 50 V for (a) 0.0068M and (b) 0.0076M. Other than 0.0068 and 0.0076M samples, no samples showed significant current.

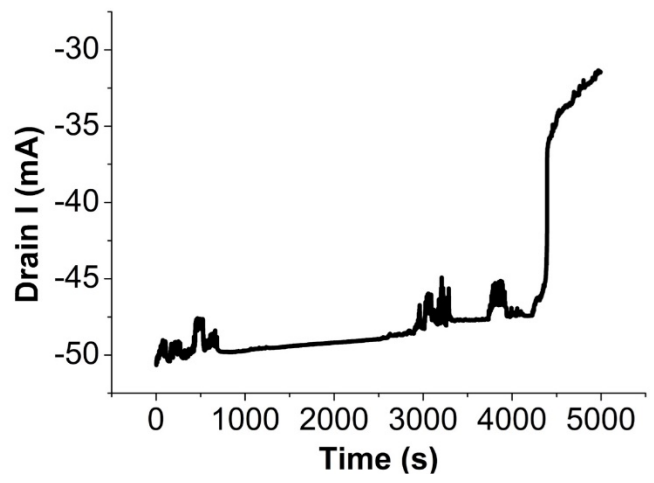


Figure 8. Timed test of 0.0076M peptide sample for 5000s under - 0.5 V bias. The current remained relatively stable until rapid degradation after about 4000s, leading to about 40 % degradation/60% retention in current output after 5000s.

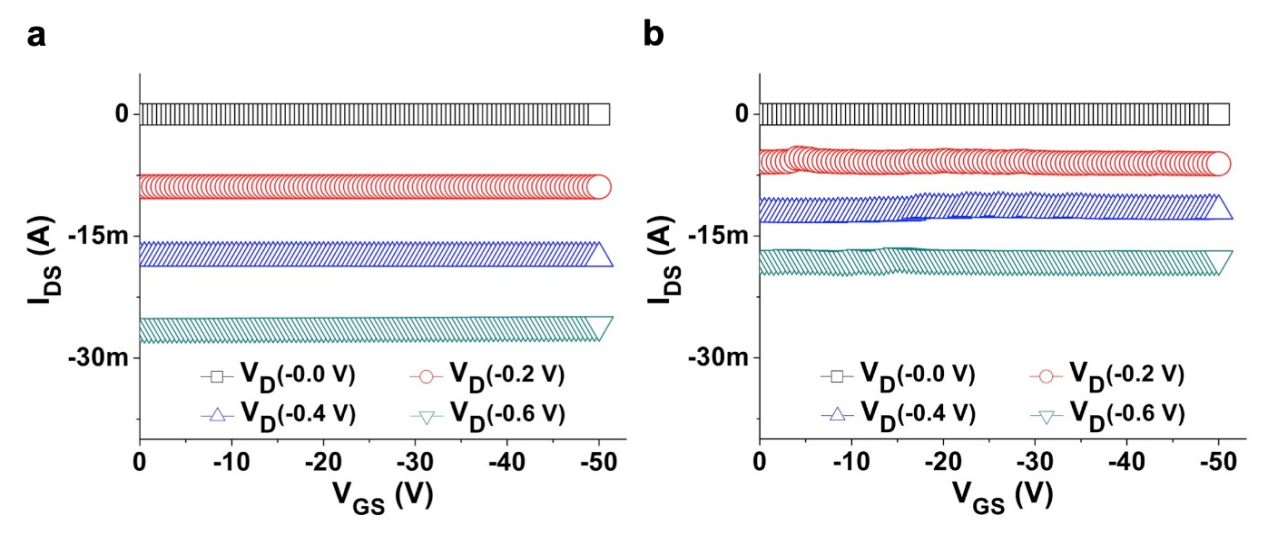


Figure 9. Currents over V_{GS} range of 0.0076M peptide sample after 20 days since fabrication. (a) Before exposure to ammonium hydroxide. (b) After exposure to ammonium hydroxide for 5 minutes.

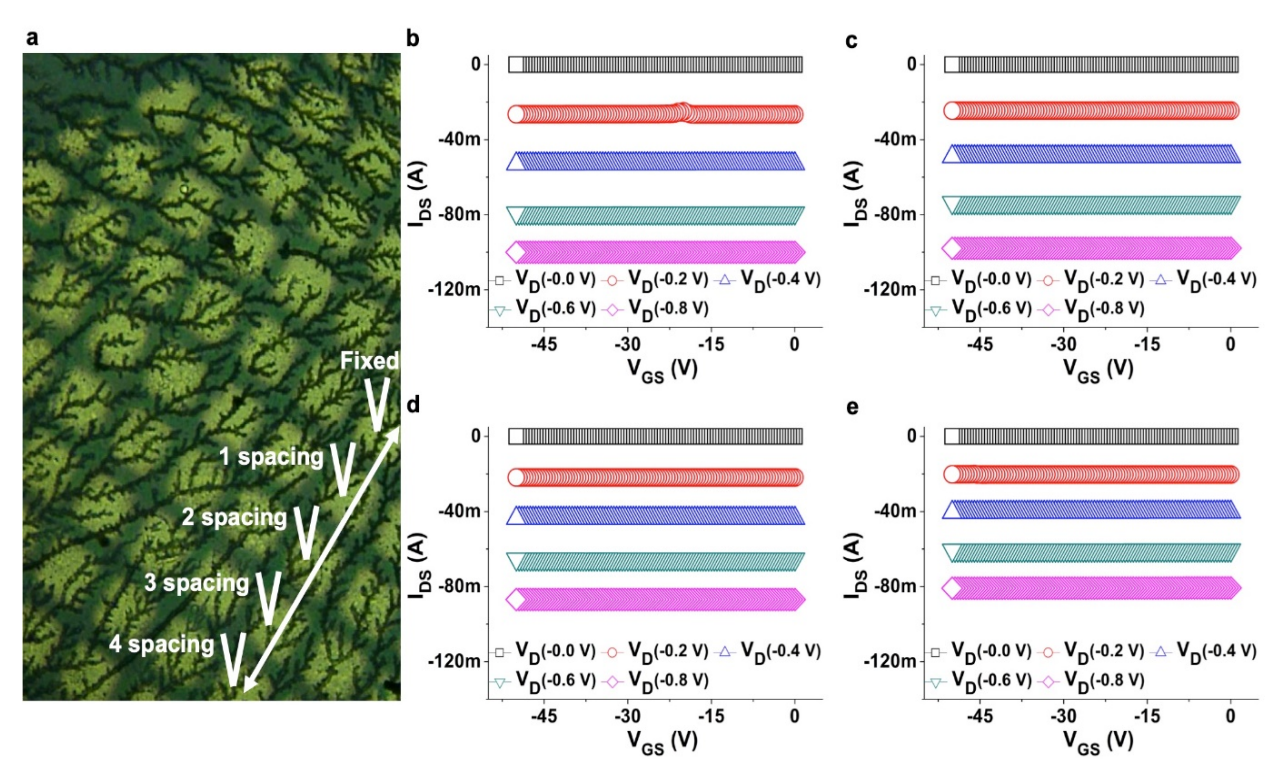


Figure 10. Spacing test measuring current of 0.0076M peptide sample for different number of spacing between electrodes. (a) 10x microscope image showing electrodes used for each respective spacing measurement. Currents over V_{GS} range forelectrodes with (b) 1 spacing, (c) 2 spacing, (d) 3 spacing, and (e) 4 spacing.

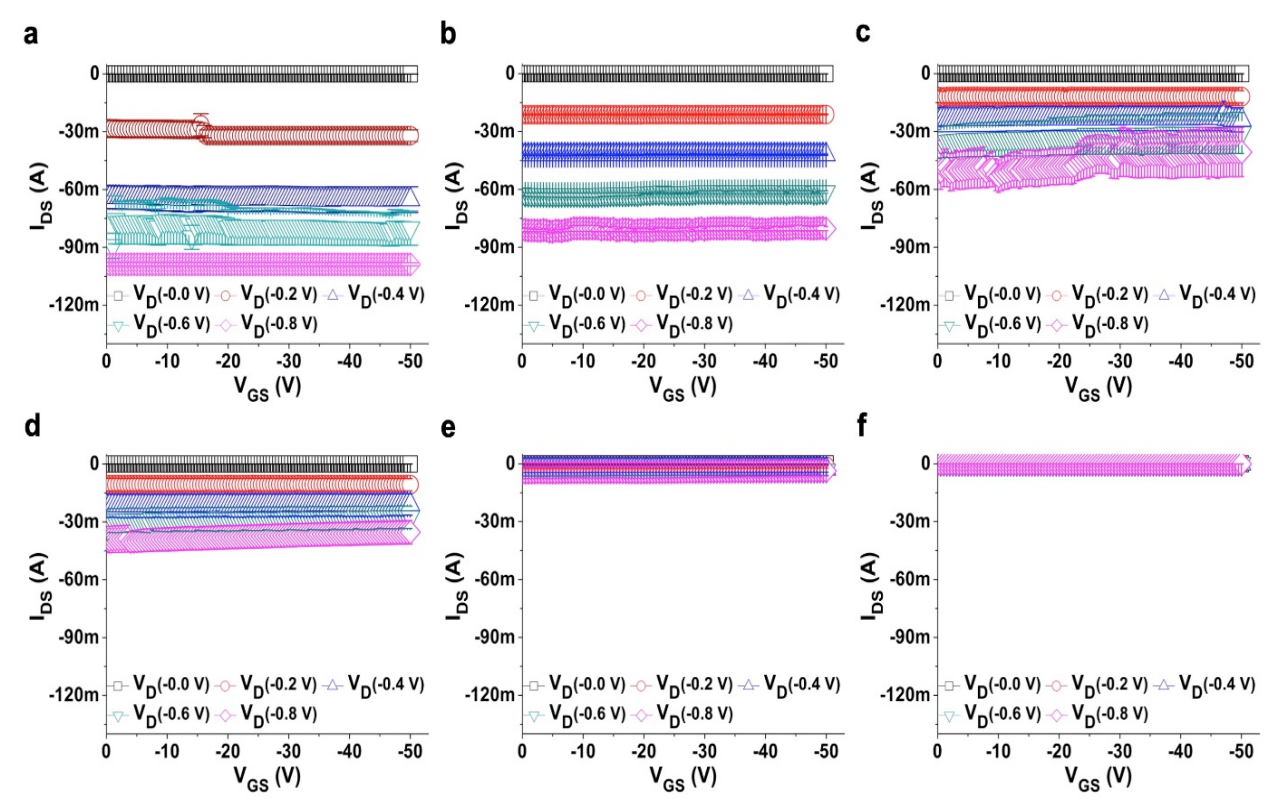


Figure 11. Shelf life test using plots of Currents over V_{GS} range of 0.0076M peptide sample for (a) 3 days, (b) 6 days, (c) 12 days, (d) 18 days, (e) 43 days, (f) 146 days.

Table of Contents Graphic

